Nonlocal correlations in quantum energy teleportation: Perspectives from their Majorana representations and information thermodynamics

Hiroaki Matsueda,[1,2,*] Yusuke Masaki,[1] Kanji Itoh,[1] Atsushi Ono,[3] and Joji Nasu[3]
[1]*Department of Applied Physics, Graduate School of Engineering, Tohoku University, Sendai 980-8579, Japan*
[2]*Center for Science and Innovation in Spintronics, Tohoku University, Sendai 980-8577, Japan*
[3]*Department of Physics, Graduate School of Science, Tohoku University, Sendai 980-8578, Japan*

(Received 7 December 2024; accepted 23 July 2025; published 8 August 2025)

Motivated by anomalous nonlocal correlation in the Kitaev spin liquids, we propose a quantum energy teleportation protocol between remote partners Alice and Bob on a quantum spin model, and examine how its performance is characterized by Majorana fermions that clearly depict nonlocal correlations inherent in the model. In our model, Bob's energy extraction is activated by energy injection by Alice's projective measurement and subsequent classical communication of the measurement result. We derive two formulas: one for the maximally extracted energy by the protocol, $\Delta E_B^{\max}$, and the other for the maximum of energy reduction in a local spin system where Bob performs feedback unitary operation, $\Delta E_{B,B}^{\max}$. The protocol aims to extract a positive amount of the former energy distinct from the latter due to the presence of an interaction between the local system and others. We find that the extracted energy becomes positive when a nonlocal correlator defined by Majorana fermions at Alice and Bob's sites is finite. We also find that the amount of the energy reduction becomes positive when another nonlocal Majorana correlator is finite. In both formulas, the correlators appear as a result of Bob's feedback unitary operation. We find that the latter formula is equal to the upper bound of energy extraction in the second law of effective information thermodynamics. We discuss the effective information-thermodynamical aspects behind the protocol at zero temperature.

DOI: 10.1103/1yr5-sn98

I. INTRODUCTION

Quantum teleportation transfers quantum information (or a quantum state) to a distant place by using an entanglement pair and projective measurement. Quantum teleportation is thus the most fundamental protocol for quantum communication technologies, and nearly 30 years have passed since this protocol was developed [1]. Quantum teleportation provides meaningful perspectives not only in the field of communication technologies, but also in recent research on traversable wormholes in spacetime physics and its holographic realization on quantum processors [2–5].

Phenomena similar to quantum teleportation can also be seen in solid-state physics, although the transportation range seems to be of microscopic scale. Nice playgrounds are Kitaev quantum spin systems. The Kitaev model is an exactly solvable quantum spin model, whose ground state is a quantum spin liquid with elementary excitations described by Majorana fermions [6–13]. Two related studies have been conducted in recent years. The first one is about detection of the magnetic moment at one edge of the Kitaev model after pulse magnetic excitation to the opposite edge [14–18]. The second one is about long-range correlation between two remote impurities introduced in the Kitaev model [19]. In both cases, there is no direct transportation of spin waves. Instead, the Majorana physics is a key for understanding such long-range correlations. In addition, performing braiding operations of Majorana zero modes is a candidate for teleportation-based quantum information processing [20–22]. Thus, the physics of Majorana fermions has good connection with quantum teleportation theories and technologies.

Unfortunately, the abovementioned two studies do not directly consider how each physical process and the long-range correlation correspond to traditional quantum teleportation protocols. In the protocol, any nonlocal correlation function between an information sender and receiver does not appear. In order to understand the roles of the Majorana correlations on the teleportationlike behaviors in the Kitaev systems, we consider quantum energy teleportation (QET) rather than quantum teleportation [23–32]. As shown later, this research is also related to a very fundamental question about the second law of information thermodynamics, which is how work extraction is enhanced by quantum information [33–39].

Motivated by these cross-disciplinary interests, we examine a QET protocol for remote partners Alice and Bob on the ground state of a one-dimensional quantum spin model that is transformed into a model of Majorana fermions. In a basic assumption of the QET protocol, Alice and Bob perform local operations and classical communication at a speed much faster than that of any physical mode. Thus, this

*Contact author: hiroaki.matsueda.c8@tohoku.ac.jp

Published by the American Physical Society under the terms of the Creative Commons Attribution 4.0 International license. Further distribution of this work must maintain attribution to the author(s) and the published article's title, journal citation, and DOI.

protocol does not require a direct physical connection between Alice and Bob except for ground-state entanglement. In this situation, Bob's feedback unitary transformation activates energy extraction after energy injection by Alice's projective measurement. We would like to understand how nonlocal Majorana correlation facilitates the positive energy extraction using the QET protocol.

The relation between extracted energy and a two-point correlator connecting Alice and Bob's spins has already been obtained from early QET research [23]. This result helps us to examine the Majorana correlation in our research. Nonlocal correlation and entanglement are closely related concepts, and the study of energy-entanglement relation may be important. However, the energy-entanglement relation studied in the minimal QET model is given as inequalities with complicated factors, and the proof method lacks extensibility to proofs in other models [26]. The role of entanglement in our QET model will be shown to manifest in a different form.

Using the Majorana representations of nonlocal correlators makes the physical meaning of the QET performance clearer in our model. This result is the first advantage of our QET research. We will derive the first formula to represent the relation between the extracted energy and a nonlocal Majorana correlator. In our model, Bob's feedback unitary operation for the energy extraction is defined locally, but the extracted energy is not a local quantity because of the interaction between Bob's local spin and the other part. In this case, we would also like to focus on energy reduction at Bob's local site. We will derive the second formula that relates another nonlocal Majorana correlator to the local energy reduction. These nonlocal Majorana correlators appear as a result of Bob's feedback operation, and contribute to the energy extraction or the local energy reduction. The difference between the amount of the local energy reduction and the extracted energy corresponds to the energy that could hinder the performance of energy extraction. We will find that the Majorana representation of a three-point correlator appearing in the formula of the energy difference does not show a connection between Majorana fermions at Alice and Bob's sites.

The second advantage of our QET research is that it provides very useful perspectives for deepening thermodynamics. As already mentioned, the energy difference could hinder the QET performance for energy extraction. We will find that the energy difference is finite in general and becomes zero for the QET process that maximizes the extractable energy. We will find that the second energy formula is consistent with our recent result on the upper bound on locally extractable energy from an entangled pure state under feedback control [39]. We will find that the nonlocal Majorana correlator related to the local energy reduction is different from the quantum-classical (QC) mutual information appearing in our previous work [39], although both of the Majorana correlator and the QC-mutual information are quantum-information resources for driving these protocols.

This paper is organized as follows. In the next section, we introduce our model, and represent it using Jordan-Wigner fermions. In Sec. III, we explain our QET protocol, and derive the formulas of the extracted energy and the local energy reduction. In Sec. IV, we derive the Majorana fermion representations of these formulas, and discuss the roles of the nonlocal Majorana correlations on these formulas. Section V is devoted to the discussion about the first and second laws of effective information thermodynamics inherent in the present model. On the basis of the present result, we summarize our results in Sec. VI. In Appendix A, the symmetry operations to determine the ground-state properties are provided. In Appendix B, mathematical details for deriving the maxima of the extracted energy and the local energy reduction are provided. In Appendix C, the effect of the degeneracy of even- and odd-parity states on the QET performance is provided. The derivations of some equations are also provided in Appendixes D and E.

II. MODEL

The QET protocol is as follows: First, the ground state with quantum entanglement is prepared, and Alice makes a local measurement at one endpoint of the system. Next, the measurement result is transmitted to Bob, at the opposite endpoint, via a classical communication channel. Then, Bob performs a local feedback unitary operation based on the result. Alice injects energy into the system by the measurement. Bob can extract energy from the system by the unitary operation. It is assumed that Alice's classical communication and Bob's manipulation are sufficiently faster than the transmission rate of elementary excitation that can occur after Alice's measurement.

Let us start with the Hamiltonian defined by

$$H = H_A + H_V + H_B, \tag{1}$$

$$H_A = h\sigma_A^z, \tag{2}$$

$$H_V = k\left(\sigma_A^x\sigma_{C_1}^x + \sigma_{C_1}^y\sigma_{C_2}^y + \sigma_{C_2}^x\sigma_B^x\right), \tag{3}$$

$$H_B = h\sigma_B^z, \tag{4}$$

where σ_i^α ($\alpha = x, y, z$) is the Pauli operator at site i (the site indices, A, C_1, C_2, and B, are sometimes replaced with 0, 1, 2, and 3, respectively). The model contains four spins A, C_1, C_2, and B, and their spatial geometry is illustrated in Fig. 1. The interaction strength k creates entanglement, and the edge magnetic field h controls the amount of the entanglement. The interaction term has a special form so that our model matches with the analysis of Majorana correlation in the Kitaev spin liquids. This point will be discussed in Sec. IV. We will apply the local operation and classical communication to this ground state.

For later convenience to discuss Majorana correlation, we introduce the Jordan-Wigner transformation to spin operators: $\sigma_i^z = 2f_i^\dagger f_i - 1$, $\sigma_i^x = \Theta_i(f_i^\dagger + f_i)$, $\sigma_i^y = -i\Theta_i(f_i^\dagger - f_i)$, and $\Theta_i = e^{i\pi\sum_{l(<i)} f_l^\dagger f_l} = \prod_{l(<i)}(-\sigma_l^z)$, where $i = 0, 1, 2, 3$ (A, C_1, C_2, B), $f_i^\dagger$ and f_i are the creation and annihilation operators of the Jordan-Wigner fermion at site i, respectively, and Θ_i is the string operator ($\Theta_0 = 1$). Hereafter, we abbreviate $\Theta_3(=\Theta_B)$ as Θ. The interaction term is transformed into the following form: $H_V = k(f_A^\dagger - f_A)(f_{C_1}^\dagger + f_{C_1}) - k(f_{C_1}^\dagger + f_{C_1})(f_{C_2}^\dagger - f_{C_2}) + k(f_{C_2}^\dagger - f_{C_2})(f_B^\dagger + f_B)$.

The Jordan-Wigner-fermion representation of the Hamiltonian shows that the operation that swaps the parity of the

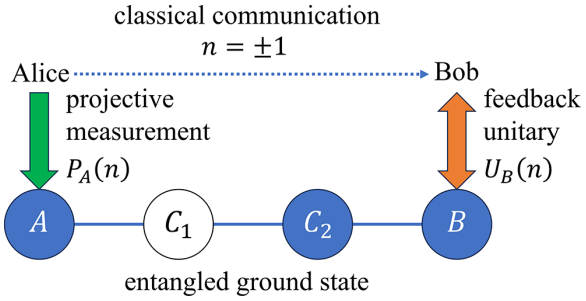


FIG. 1. Illustration of our four-spin model and protocol. Alice and Bob perform local projective measurement $P_A(n)$ to spin A and local feedback unitary operation $U_B(n)$ to spin B, respectively. The green arrow represents energy injection by the measurement, and the orange arrow represents energy injection or extraction depending on the selection of the unitary operator. The classical communication between Alice and Bob is indicated by the dotted arrow, and the measurement results are $n = \pm 1$. The final result for the extracted energy is represented by the operators defined at sites A, C_2, and B (blue shaded circles).

fermion number is forbidden. Therefore, each eigenstate belongs to the subspace of either even or odd fermion number. Figure 2 shows the h dependence of the eigenvalue spectra E of H in the even-parity sector that is spanned by even numbers of Jordan-Wigner fermions. The eigenvalue spectra are degenerate with those in the odd-parity sector that is spanned by odd numbers of Jordan-Wigner fermions (see Appendix A). We find symmetry between negative and positive spectra. We also find twofold degeneracies for all of the eigenstates in each parity sector for $h = 0$, and the degeneracies are lifted by introducing finite h values. In Appendix A, we summarize symmetry operations associated with these spectroscopic properties.

As a playground of QET, we prepare the lowest-energy eigenstate $|\psi\rangle$ in the even-parity sector. The corresponding

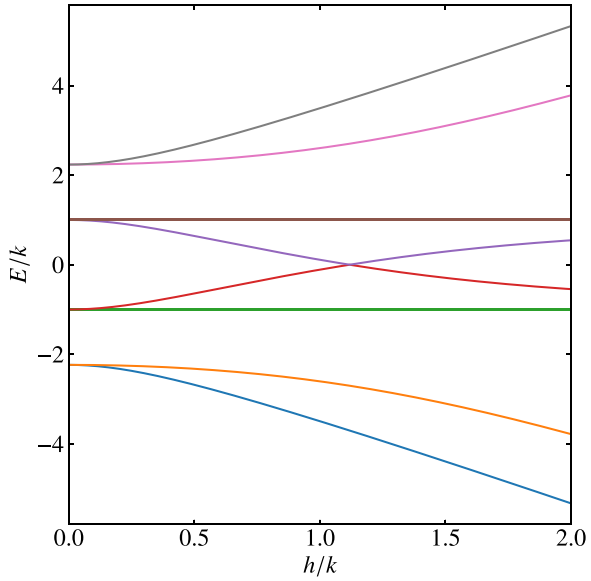


FIG. 2. Eigenvalue spectra E in the even-parity sector as a function of h. The initial-state energy of our QET is denoted as the blue solid line.

energy eigenvalue is represented as ϵ ($H|\psi\rangle = \epsilon|\psi\rangle$). According to symmetry restriction shown in Appendix A, the state $|\psi\rangle$ for $h \geqslant 0$ is represented as

$$|\psi\rangle = Z[(|eeff\rangle + |efef\rangle) + \alpha(|ffff\rangle + |feef\rangle) + (|ffee\rangle + |fefe\rangle) + \beta(|eeee\rangle + |effe\rangle)], \quad (5)$$

where $|eeff\rangle = f^\dagger_{C_2} f^\dagger_B |eeee\rangle$, $|eeee\rangle = |e\rangle_A \otimes |e\rangle_{C_1} \otimes |e\rangle_{C_2} \otimes |e\rangle_B$, $|eeee\rangle$ is the vacuum of the Jordan-Wigner fermions, and $\sigma^z_i|e\rangle_i = -|e\rangle_i$, $\sigma^z_i|f\rangle_i = |f\rangle_i$ with $i = A, C_1, C_2, B$. The normalization factor Z is determined by $(4 + 2\alpha^2 + 2\beta^2)Z^2 = 1$. By substituting Eq. (5) into the eigenvalue equation $H|\psi\rangle = \epsilon|\psi\rangle$, we find that the parameters, α and β, and the lowest eigenvalue ϵ are related as $\alpha = 2k/(\epsilon + k - 2h)$, $\beta = 2k/(\epsilon + k + 2h)$, and $\epsilon = k(\alpha + \beta + 1)$. By combining these equations together, we find that ϵ is determined by solving the following equation:

$$(\epsilon + k)(\epsilon^2 - 5k^2) - 4h^2(\epsilon - k) = 0. \quad (6)$$

We find that $\lim_{h\to 0} \epsilon = -\sqrt{5}k$ and $\epsilon < -\sqrt{5}k$ for $h > 0$ as shown in Fig. 2. We can derive $\alpha\beta = (\epsilon - k)/(\epsilon + k) > 0$ for general h values. The expectation value of H_i ($i = A, V, B$) by $|\psi\rangle$ is represented as $\epsilon_i = \langle\psi|H_i|\psi\rangle$, and their sum is equal to the eigenvalue $\epsilon = \epsilon_A + \epsilon_V + \epsilon_B$. We find $\epsilon_A = 2hZ^2(\alpha^2 - \beta^2) \leqslant 0$ and $\epsilon_A = \epsilon_B$. For later convenience, we introduce the following representation for H_V: $H_V = H_L + H_C + H_R$, $H_L = k\sigma^x_A\sigma^x_{C_1}$, $H_C = k\sigma^y_{C_1}\sigma^y_{C_2}$, and $H_R = k\sigma^x_{C_2}\sigma^x_B$. Their expectation values are also represented as $\epsilon_i = \langle\psi|H_i|\psi\rangle$ ($i = L, C, R$). We find $\epsilon_L = 4kZ^2(\alpha + \beta) < 0$ and $\epsilon_L = \epsilon_R$.

For $h = 0$, $|\psi\rangle$ is factorized into the following form: $|\psi\rangle = Z|fe - ef\rangle_{AB} \otimes |fe + ef\rangle_{C_1C_2} + Z\alpha|ff + ee\rangle_{AB} \otimes |ff + ee\rangle_{C_1C_2}$, where we have rearranged the order of the basis states, and $|ff + ee\rangle_{AB} = |f\rangle_A \otimes |f\rangle_B + |e\rangle_A \otimes |e\rangle_B$. It is clear that the local states at Alice and Bob's sites are correlated with each other. This correlation characterizes long-range entanglement in this model at least for $h = 0$.

III. PROTOCOL

Let us introduce Alice's measurement and Bob's feedback unitary operations in our QET protocol as already indicated in Fig. 1. Alice makes the following local measurements on spin A:

$$P_A(n) = \tfrac{1}{2}(I_A + n\vec{r}\cdot\vec{\sigma}_A), \quad (7)$$

where the measurement result n takes ± 1, I_A is the identity operator, $\vec{r} = (r_x, r_y, r_z)$ is a unit vector, and $P^2_A(n) = P_A(n)$. Alice sends the measurement result n to Bob by the classical communication channel. Depending on the result n, Bob performs the following feedback unitary operation on spin B:

$$U_B(n) = e^{in\theta\vec{s}\cdot\vec{\sigma}_B} = I_B\cos\theta + in\vec{s}\cdot\vec{\sigma}_B\sin\theta, \quad (8)$$

where $\vec{s} = (s_x, s_y, s_z)$ is a unit vector. For $\theta \neq 0, \pm\pi/2$, the feedback unitary operation is realized.

We evaluate the injected energy by Alice's measurement, $\Delta E_A = E_A - \epsilon$, where E_A is the energy expectation value after Alice's measurement: $E_A = \sum_{n=\pm 1}\langle\psi|P_A(n)HP_A(n)|\psi\rangle$. Here, the quantum state after Alice's measurement is represented as $|\psi_A(n)\rangle = P_A(n)|\psi\rangle/\sqrt{\langle\psi|P_A(n)|\psi\rangle}$, and the form of E_A is reduced to $E_A = \sum_{n=\pm 1} p_n\langle\psi_A(n)|H|\psi_A(n)\rangle$, where

$p_n = \langle\psi|P_A(n)|\psi\rangle$ is the probability of obtaining a measurement result n. The energy E_A is evaluated as $E_A = r_z^2\epsilon_A + r_x^2\epsilon_L + \epsilon_C + \epsilon_R + \epsilon_B$, and the injected energy, ΔE_A, is given by

$$\Delta E_A = \big(r_z^2 - 1\big)\epsilon_A + \big(r_x^2 - 1\big)\epsilon_L. \tag{9}$$

It is clear that Alice's measurement injects positive energy ($\Delta E_A > 0$) into the vicinity of spin A. Due to the interaction H_L between two spins A and C_1, Eq. (9) includes ϵ_L as well as ϵ_A.

We also introduce the energy expectation value after Bob's feedback unitary operation: $E_B = \sum_{n=\pm1}\langle\psi|P_A(n)U_B^\dagger(n)HU_B(n)P_A(n)|\psi\rangle = r_z^2\epsilon_A + r_x^2\epsilon_L + \epsilon_C + \sum_{n=\pm1}\langle\psi|P_A(n)U_B^\dagger(n)(H_B + H_R)U_B(n)|\psi\rangle$. The energy extracted by Bob's operation, $\Delta E_B = E_A - E_B$ (the energy extraction occurs when $\Delta E_B > 0$), is given by the sum of two contributions:

$$\Delta E_B = \Delta E_{B,B} + \Delta E_{B,R}, \tag{10}$$

where

$$\Delta E_{B,i} = \epsilon_i - \sum_{n=\pm1}\langle\psi|P_A(n)U_B^\dagger(n)H_iU_B(n)|\psi\rangle, \tag{11}$$

with $i = B, R$. The extracted-energy formula, ΔE_B, contains H_B and H_R. Thus, the energy is extracted from the vicinity of spin B, and the interaction H_R is included as in the case of energy injection. The quantity $\Delta E_{B,B}$ only includes H_B, and corresponds to the reduction of internal energy of Bob's local spin. We have confirmed that Eqs. (10) and (11) hold regardless of the details of H_C under the constraint that H_C commutes with $P_A(n)$ and $U_B(n)$, since ϵ_C disappears by subtracting E_A and E_B [23]. The second term in the right-hand side (RHS) of Eq. (11) corresponds to nonlocal correlation between Alice's measurement operator $P_A(n)$ and the operator $U_B^\dagger(n)H_iU_B(n)$ that is associated with Bob's feedback operation. The quantities $\Delta E_{B,B}$ and $\Delta E_{B,R}$ are evaluated as follows:

$$\begin{aligned}\Delta E_{B,B} =& \epsilon_B\big(1 - s_z^2\big)(1 - \cos(2\theta)) \\ &- h(r_x s_y C_{AB} - r_y s_x D_{AB})\sin(2\theta),\end{aligned} \tag{12}$$

$$\Delta E_{B,R} = \epsilon_R\big(1 - s_x^2\big)(1 - \cos(2\theta)) + k r_x s_y C_{AR}\sin(2\theta), \tag{13}$$

where the two-point correlators, C_{AB} and D_{AB}, are, respectively, defined by

$$C_{AB} = \langle\psi|\sigma_A^x\sigma_B^x|\psi\rangle = 4Z^2(1 + \alpha\beta), \tag{14}$$

$$D_{AB} = \langle\psi|\sigma_A^y\sigma_B^y|\psi\rangle = 4Z^2(1 - \alpha\beta), \tag{15}$$

and the three-point correlator, C_{AR}, is defined by

$$C_{AR} = \langle\psi|\sigma_A^x\sigma_{C_2}^x\sigma_B^z|\psi\rangle = 4Z^2(\alpha - \beta). \tag{16}$$

For $h \to 0$ ($\alpha = \beta$ and $\alpha\beta = (3 + \sqrt{5})/2 > 1$), we find $C_{AB} = 1$, $D_{AB} < 0$, and $C_{AR} = 0$. In order to achieve $\Delta E_B = \Delta E_{B,B} + \Delta E_{B,R} > 0$, at least either $\Delta E_{B,B}$ or $\Delta E_{B,R}$ must be positive. Since the first terms in Eqs. (12) and (13) are always negative, their second terms are essential to $\Delta E_B > 0$. The second terms are finite values for the feedback operation ($\theta \neq 0, \pm\pi/2$), at which nonlocal correlations C_{AB}, D_{AB}, and C_{AR} appear.

Let us mention what happens if Bob does not receive Alice's signal. This can be achieved by replacing $U_B(n)$ with a unitary operation without feedback, u_B ($=U_B(+1)$ or $U_B(-1)$), in Eq. (11). We find $\Delta E_{B,B} = \epsilon_B - \sum_{n=\pm1}\langle\psi|P_A(n)u_B^\dagger H_B u_B|\psi\rangle = \epsilon_B(1 - s_z^2)(1 - \cos(2\theta))$ and $\Delta E_{B,R} = \epsilon_R - \sum_{n=\pm1}\langle\psi|P_A(n)u_B^\dagger H_R u_B|\psi\rangle = \epsilon_R(1 - s_x^2)(1 - \cos(2\theta))$. Here, the absence of n dependence of u_B leads to cancellation of the effect of Alice's measurement $\sum_n P_A(n) = 1$. The results support our statement that the feedback control induces the effects of the nonlocal correlations on $\Delta E_{B,B}$ and $\Delta E_{B,R}$.

By optimizing $\vec{r}$, $\vec{s}$, and θ (see Appendix B), we obtain the maximum of ΔE_B [23], denoted by $\Delta E_B^{\max}$, as

$$\Delta E_B^{\max} = \sqrt{\epsilon_B^2 + (hD_{AB})^2} - |\epsilon_B|, \tag{17}$$

where the optimization conditions are given by $\vec{r} = (0, 1, 0)$, $\vec{s} = (1, 0, 0)$, $\sin(2\theta) = hD_{AB}/\sqrt{\epsilon_B^2 + (hD_{AB})^2}$, and $\cos(2\theta) = -\epsilon_B/\sqrt{\epsilon_B^2 + (hD_{AB})^2}$. For the parameters that maximize ΔE_B, we find

$$\Delta E_{B,R} = 0, \tag{18}$$

and thus $\Delta E_{B,B} = \Delta E_B^{\max}$. The results show that a part of the second term in Eq. (12), $hr_y s_x D_{AB}\sin(2\theta)$, is crucial for the positive energy extraction.

We also derive the maximum value of $\Delta E_{B,B}$, denoted by $\Delta E_{B,B}^{\max}$, which was a primary focus in our previous study [39] (see Appendix B). The maximum value is obtained as

$$\Delta E_{B,B}^{\max} = \sqrt{\epsilon_B^2 + (hC_{AB})^2} - |\epsilon_B|, \tag{19}$$

where the optimization conditions are given by $\vec{r} = (1, 0, 0)$, $\vec{s} = (0, 1, 0)$, $\sin(2\theta) = -hC_{AB}/\sqrt{\epsilon_B^2 + (hC_{AB})^2}$, and $\cos(2\theta) = -\epsilon_B/\sqrt{\epsilon_B^2 + (hC_{AB})^2}$. For the parameters that maximize $\Delta E_{B,B}$, we find

$$\Delta E_{B,R} = \epsilon_R(1 - \cos(2\theta)) + kC_{AR}\sin(2\theta) < 0. \tag{20}$$

Because of the inequality $|C_{AB}| > |D_{AB}|$, $\Delta E_{B,B}^{\max}$ is larger than $\Delta E_B^{\max}$. However, because of the negative feature of $\Delta E_{B,R}$, the maximum of ΔE_B can not be reached by optimizing $\Delta E_{B,B}$.

Figure 3(a) shows the h dependence of D_{AB} and C_{AB}, which are crucial factors for positive $\Delta E_B^{\max}$ and $\Delta E_{B,B}^{\max}$, respectively, as already shown in Eqs. (17) and (19). These correlators are large for a small-h region. Their behaviors after multiplying h show only weak-h dependence except for the small-h region. Figure 3(b) shows ΔE_A for $\vec{r} = (0, 1, 0)$ and $\vec{r} = (1, 0, 0)$, corresponding to $\Delta E_B^{\max}$ and $\Delta E_{B,B}^{\max}$, respectively, as a function of h. We first examine the h dependence of ΔE_A. The energy change by the projection measurement is mediated by the Alice's local Hamiltonian H_A. It is natural that ΔE_A increases as h increases. We next examine the h dependence of $\Delta E_B^{\max}$ and $\Delta E_{B,B}^{\max}$. Both of them are zero for $h = 0$, and start to increase with h. Further increase of h reduces their magnitudes, because the effect of hD_{AB} and hC_{AB} on $\Delta E_B^{\max}$ and $\Delta E_{B,B}^{\max}$ is smeared out by the increase of $|\epsilon_B|$ in the large-h region. We find $\Delta E_A > \Delta E_B^{\max}$ for $r_y = 1$. The ratio, $\Delta E_B^{\max}/\Delta E_A$ is about 0.032 for $h = 0.18k$ that is a peak position of $\Delta E_B^{\max}$. We also find $\Delta E_A > \Delta E_{B,B}^{\max}$ for $r_x = 1$ and $h > 0.24k$. The inequality is reversed for $h < 0.24k$. We

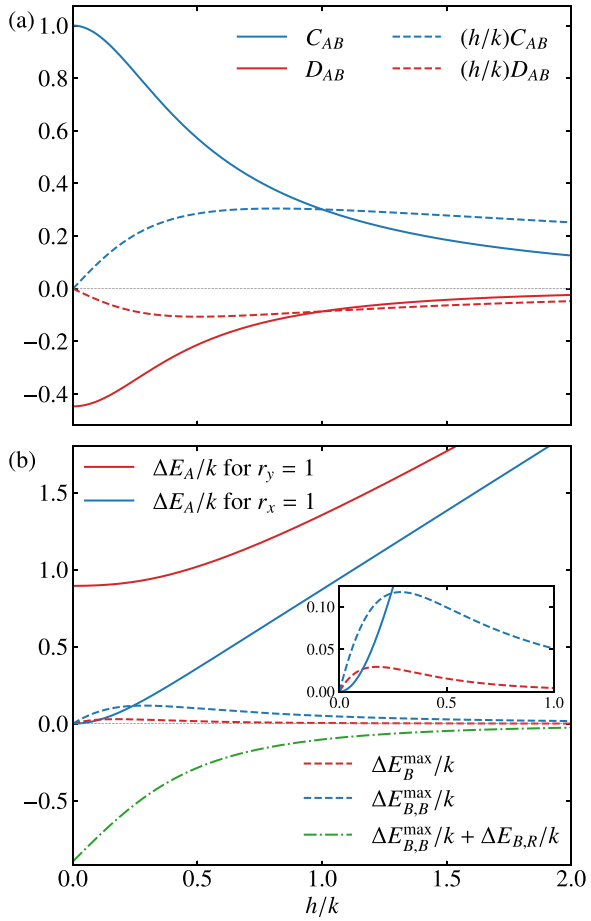


FIG. 3. (a) Nonlocal correlators C_{AB} and D_{AB} (hC_{AB} and hD_{AB}) as a function of h. (b) The red solid and dashed lines correspond to ΔE_A and ΔE_B, respectively, in the case that ΔE_B is maximized. The blue solid line corresponds to ΔE_A in the case that $\Delta E_{B,B}$ (blue dashed line) is maximized. In the latter case, ΔE_B is represented by the sum of Eqs. (19) and (20), and shows a negative value represented by the green dashed-dotted line. The inset shows a magnified view for $h < k$.

plot ΔE_B as the green dash-dotted line in Fig. 3(b) when $\Delta E_{B,B}$ is maximized. This quantity is given by the sum of Eqs. (19) and (20). We find that the quantity is negative and $|\Delta E_{B,R}| \gg \Delta E_{B,B}^{\max}$. Therefore, even if the amount of reduction in the internal energy for $h < 0.24k$ is greater than the amount of energy injected into the system, the energy to be taken out of the system does not exceed the amount of energy injected.

IV. MAJORANA FERMION REPRESENTATION OF NONLOCAL CORRELATORS

Our main purpose of this paper is to convert the present QET model into a Majorana fermion model so that we examine the relationship between QET and Majorana nonlocal correlation. The conversion is realized by introducing the following Majorana representation: $b_l = f_l^\dagger + f_l$, $c_l = i(f_l^\dagger - f_l)$, $c_m = f_m^\dagger + f_m$, and $b_m = i(f_m^\dagger - f_m)$, for $l = A, C_2$ and $m = C_1, B$. Then, the QET Hamiltonian is mapped onto the following form:

$$H = ihb_Ac_A - ik(c_Ac_{C_1} - c_{C_1}c_{C_2} + c_{C_2}c_B) + ihc_Bb_B. \quad (21)$$

For $h = 0$, the Hamiltonian is described by the bilinear form of itinerant c-Majorana fermions, and b-Majorana fermions are zero modes. The introduction of a finite h value induces coupling between c- and b-Majorana fermions at both edges. Let us compare this model with the conventional Kitaev model defined on a two-dimensional honeycomb lattice: $H = \sum_{\langle i,j\rangle_a} J_a\sigma_i^a\sigma_j^a$, where $\langle i, j\rangle_a$ represents the sum over nearest-neighbor pairs connected by an a-bond (each vertex in the honeycomb lattice has three bonds, and we label them $a = x, y, z$). By the transformation $\sigma_j^a = ib_j^ac_j$, the Hamiltonian is mapped onto an itinerant c-Majorana fermion system coupled to Z_2 gauge fields $u_{ij}^a = ib_i^ab_j^a$. The introduction of magnetic field induces coupling between b- and c-Majorana fermions. Although the transformation from spin operators to Majorana operators in our model is different from that in the Kitaev model, a correspondence between these two models can be observed as follows: the Majorana hopping with J_a in the Kitaev model corresponds to the k term in Eq. (21). The Zeeman-field term in the Kitaev model is usually represented as $-\sum_a h_a\sigma_j^a = -\sum_a ih_ab_j^ac_j$ at site j, and this representation corresponds to the edge-field term in Eq. (21). Thus, our model can be viewed as one-dimensional simplification of the Kitaev model with edge magnetic fields [14–18]. In the previous work [19], the Kitaev model with two vacancies under a magnetic field is examined. In this case also, the b-c hopping terms of the nearest-neighbor sites of the vacancies appear, when we treat the magnetic field perturbatively.

We focus on the Majorana correlation, $\langle\psi|ib_Ab_B|\psi\rangle$, that is evaluated as $\langle\psi|ib_Ab_B|\psi\rangle = -4Z^2(1 + \alpha\beta)$, which reminds us of C_{AB} in Eq. (14). In order to clarify the reason for their equivalence except for the sign, the operator product ib_Ab_B before taking the expectation value is evaluated as $ib_Ab_B = \sigma_A^x(\sigma_A^z\sigma_{C_1}^z\sigma_{C_2}^z)(i\sigma_B^y) = \sigma_A^x\sigma_B^x(-P)$, where P $(= \sigma_A^z\sigma_{C_1}^z\sigma_{C_2}^z\sigma_B^z)$ is the parity operator. For the even-parity state $|\psi\rangle$ $(P|\psi\rangle = |\psi\rangle)$, we actually obtain

$$\langle\psi|ib_Ab_B|\psi\rangle = \langle\psi|\sigma_A^x\sigma_B^x(-1)|\psi\rangle = -C_{AB}. \quad (22)$$

For the odd-parity sector, see Appendix C. We also consider the Majorana representation of D_{AB} and C_{AR}. The results are given by

$$D_{AB} = \langle\psi|ic_Ac_BP|\psi\rangle = \langle\psi|ic_Ac_B|\psi\rangle, \quad (23)$$

$$C_{AR} = \langle\psi|ib_Ac_{C_2}P|\psi\rangle = \langle\psi|ib_Ac_{C_2}|\psi\rangle. \quad (24)$$

The quantity C_{AB} (D_{AB}) represents correlation between the b-Majorana (c-Majorana) fermions at both edges. These correlators, C_{AB} and D_{AB}, appear as a result of feedback control after classical communication between Alice and Bob, and are important for maximizing $\Delta E_{B,B}$ and ΔE_B, respectively. On the other hand, the correlator C_{AR} in $\Delta E_{B,R}$ is less important for the energy extraction. In particular, $\Delta E_{B,R}$ disappears for the maximization of ΔE_B. The Majorana representation of C_{AR} does not contain information about Majorana fermions at Bob's site, even though the original representation in Eq. (16) contains the spin operator σ_B^z at Bob's site. Therefore, we consider that the Majorana representation is a nice benchmark of what kind of nonlocal correlators are important for the

maximum energy extraction and the maximum local-energy reduction.

V. ON THE SECOND LAW OF EFFECTIVE INFORMATION THERMODYNAMICS

Let us discuss effective information-thermodynamical aspects behind the present QET model. Equation (10) is suggestive for considering the energy that is difficult to control directly with Bob's local unitary operation. In order to relate Eq. (10) to our effective thermodynamics, we consider that spin B is the system for work extraction and that two spins C_1 and C_2 behave as an environment (after Alice's projective measurement, spin A has been separated from the environment). The former statement about the system is natural for the operational definition of work, since energy extraction is triggered by Bob's feedback unitary operation $U_B(n)$ and this operation is performed locally on spin B. We call ΔE_B work, since ΔE_B is extracted from the vicinity of spin B and utilized externally. Due to the presence of H_R, ΔE_B itself is not a local quantity. Let us denote the work that spin B obtains from the outside of the whole system as $W = -\Delta E_B$ and the increase in the internal energy of spin B as $\Delta U = -\Delta E_{B,B}$. Then, Eq. (10) shows that the difference between ΔU and W is given by $\Delta E_{B,R}$. The performance of work extraction is affected by $\Delta E_{B,R}$. We find that $\Delta E_{B,R}$ is zero when ΔE_B is maximized. In this case, $U_B(n)$ commutes with H_R.

It is also a natural question to ask how Eq. (19) relates to the upper bound of energy extraction in the second law of effective information thermodynamics [39]. The nonlocal correlator C_{AB} is a crucial source to maximize $\Delta E_{B,B}$, and appears in Eq. (19) as a result of Bob's feedback operations. Therefore, the appearance of C_{AB} is specific to information-thermodynamic operations. However, C_{AB} is different from the QC-mutual information that is a resource for energy extraction by feedback control. In this section, we discuss their difference.

The second law of information thermodynamics is defined for isothermal processes at temperature T, and is given by $W_{\rm ext} \leqslant -\Delta F + T I_{\rm QC}$, where the upper bound of the work extraction $W_{\rm ext}$ contains information-gain term characterized by the QC-mutual information $I_{\rm QC}$ as well as free-energy change ΔF [33,40,41]. Motivated by the second law, some of the present authors have recently derived the upper bound on locally extractable energy from entangled pure states under feedback control [39]. The present setup matches with that of Ref. [39], when we regard H_B as the Hamiltonian of the local system of our interest (in Ref. [39], we did not consider interaction terms and there is no energy associated with $\Delta E_{B,R}$). The energy reduction $\Delta E_{B,B}$ shows the second-law-like behavior as

$$\Delta E_{B,B} \leqslant \mathcal{F}\big(\rho_B^{\rm i}; H_B\big) - F(\sigma_B) + \frac{1}{\beta_{\rm eff}} I_{\rm QC}, \tag{25}$$

where $\mathcal{F}(\rho_B^{\rm i}; H_B)$ is the nonequilibrium free energy for the reduced density matrix of the ground state $\rho_B^{\rm i} = {\rm tr}_{AC_1C_2}|\psi\rangle\langle\psi|$, $F(\sigma_B)$ is the free energy of the thermal equilibrium state for the local Hamiltonian H_B, $\sigma_B = e^{-\beta_{\rm eff} H_B}/Z_{\rm eff}$ with the partition function $Z_{\rm eff}$, and $\beta_{\rm eff}$ is an effective inverse temperature that originates in the coupling between the B site and C_1C_2 sites. Two important quantites in Eq. (25) are the free-energy difference and the QC-mutual information, $I_{\rm QC}$, respectively, defined by

$$\mathcal{F}\big(\rho_B^{\rm i}; H_B\big) - F(\sigma_B) = \frac{1}{\beta_{\rm eff}} D\big(\rho_B^{\rm i} || \sigma_B\big) \geqslant 0, \tag{26}$$

$$I_{\rm QC} = S\big(\rho_B^{\rm i}\big) - \sum_{n=\pm 1} p_n S\big(\rho_B^{\rm m}(n)\big) \geqslant 0, \tag{27}$$

where $D(\rho_B^{\rm i}||\sigma_B) = {\rm tr}_B(\rho_B^{\rm i} \log(\rho_B^{\rm i}/\sigma_B))$ denoting the Kullback-Leibler (KL) divergence, $S(\sigma) = -{\rm tr}_B(\sigma \log \sigma)$ denoting the von Neumann entropy of a density matrix σ, and $\rho_B^{\rm m}(n) = {\rm tr}_{AC_1C_2}|\psi_A(n)\rangle\langle\psi_A(n)|$. The KL divergence shows how the initial nonequilibrium state is far from σ_B, and is also an important resource of the energy reduction as well as the QC-mutual information. The equality condition of Eq. (25) holds only if the following relation is satisfied:

$$S(\sigma_B) = \min_{\{P_A(n)\}} \sum_n p_n S\big(\rho_B^{\rm m}(n)\big), \tag{28}$$

where the minimization is performed over all possible projection operators, and is realized for $\vec{r} = (1, 0, 0)$ (see Appendix D). The projection operator $P_A(n)$ for the minimization also gives the maximum value of $\Delta E_{B,B}$ in the present case. Equation (28) is used for the determination of $\beta_{\rm eff}$.

As shown in Appendix E, the RHS of Eq. (25) is equal to $\Delta E_{B,B}^{\max}$ in Eq. (19) for $\beta_{\rm eff}$ determined by Eq. (28). According to Eq. (12), $\Delta E_{B,B}^{\max}$ is the sum of $\epsilon_B(1 - \cos(2\theta))$ and $-hC_{AB}\sin(2\theta)$ for the optimized values of $\vec{r}$, $\vec{s}$, and θ. The former contribution, $\epsilon_B(1 - \cos(2\theta))$, is always negative, and then the latter contribution, $-hC_{AB}\sin(2\theta)$, is larger than the RHS of Eq. (25). The KL divergence contains information about entanglement-entropy change by the measurement, and thus not only the QC-mutual information but also the KL divergence is related to C_{AB}.

Figure 4 shows the h dependence of all components in $\Delta E_{B,B}^{\max}$ and the RHS of Eq. (25). We actually observe $-hC_{AB}\sin(2\theta) \geqslant \Delta E_{B,B}^{\max} = (D(\rho_B^{\rm i}||\sigma_B) + I_{\rm QC})/\beta_{\rm eff}$. As h increases, $D(\rho_B^{\rm i}||\sigma_B)/\beta_{\rm eff}$ tends to disappear. The decay of $D(\rho_B^{\rm i}||\sigma_B)/\beta_{\rm eff}$ is more remarkable than that of $I_{\rm QC}/\beta_{\rm eff}$. For $h/k > 1$, the RHS of Eq. (25) is almost equal to $I_{\rm QC}/\beta_{\rm eff}$. In this parameter region, $\epsilon_B(1 - \cos(2\theta))$ still remains, and this decay is slow. These data show that the nonlocal correlation term is not simply equal to the QC-mutual information even for the parameter region in which the KL divergence disappears.

VI. CONCLUDING REMARKS

We have considered QET on a quantum spin model and its Majorana representation in order to examine the roles of the Majorana correlations on the teleportation properties. We have derived the formula for connecting the maximally extracted energy $\Delta E_B^{\max}$ with the nonlocal c-Majorana correlator D_{AB}, and have shown that the correlator is necessary for the positive energy extraction. We have also derived the formula about the maximum of the local energy reduction $\Delta E_{B,B}^{\max}$ that is consistent with our previous work [39]. In this case, the nonlocal b-Majorana correlator C_{AB} is necessary for the energy reduction. In both cases, the nonlocal correlators appear as

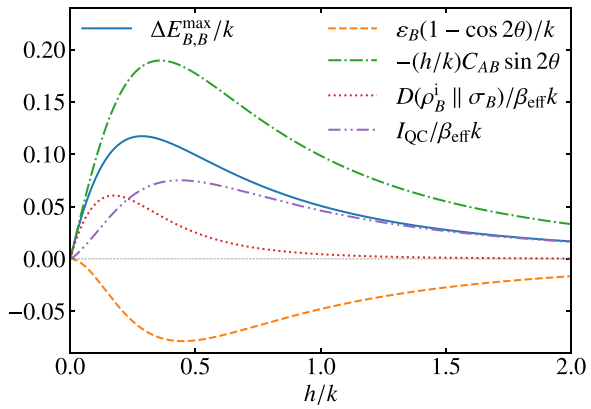


FIG. 4. Comparison among $\Delta E^{\max}_{B,B}$ (blue solid line) and its building blocks. The energy, $\Delta E^{\max}_{B,B}$, is evaluated using the RHS of Eq. (12) at the optimized values of $\vec{r}$, $\vec{s}$, and θ. The first and the second terms on the RHS of Eq. (12) under these conditions are plotted with orange dashed and green dashed-dotted lines, respectively. The free-energy change [KL divergence divided by β_{eff}, Eq. (26)] and the information-gain term [Eq. (27) divided by β_{eff}] are also plotted with red dotted and purple dashed-dotted lines, respectively, and their sum [the RHS of Eq. (25)] coincides with $\Delta E^{\max}_{B,B}$ (blue solid line) when β_{eff} is determined by Eq. (28).

a result of Bob's feedback control. We have assigned $\Delta E_{B,R}$ as energy that is difficult to control by Bob's local operation. We have found that $\Delta E_{B,R}$ is zero when the extracted energy is maximized. We have also found that the Majorana correlator C_{AB} is different from the QC-mutual information in our previous work [39], although both of the Majorana correlator and the QC-mutual information are quantum-information resources for driving these protocols.

It is an important question to ask whether $\Delta E_{B,R}$ can be regarded as heat or work from the environment (C_1C_2). This remains an unresolved issue, but it is very interesting that the problem of defining work and heat in quantum thermodynamics is involved in this research.

Equations (10) and (11) hold regardless of the details of H_C, although the values of C_{AB}, D_{AB}, and C_{AR} depend on the system size L. Thus, our statements are applicable to larger systems and systems with different geometries and spatial dimension. We have numerically evaluated those correlators for $H_C = -ik\sum_{l=0}^{L-2}(-1)^l c_l c_{l+1}$ up to $L = 1000$ in one dimension. For various L values, we have found that $C_{AB} = 1$ for $h = 0$ and C_{AB} decreases with increasing h [see also Fig. 3(a) for $L = 4$]. With increasing L, the decrease becomes stronger. For various L values, we have also found that the absolute value of D_{AB} is maximum for $h = 0$ and decreases with increasing h [see also Fig. 3(a) for $L = 4$]. The absolute value shows power-law decay as a function of L for finite-h values, which is evidence of quantum criticality of our model. The slow decay due to the power-law correlation enables us to consider QET for relatively large-L systems.

In the previous study of the Kitaev model [14], the induced magnetic moment after the pulse field excitation is measured by the time-dependent calculation. The time delay of the classical communication in the QET protocol may weaken the QET performance. It is a future work whether our statement holds in time-dependent cases.

ACKNOWLEDGMENTS

This work was supported by JSPS KAKENHI Grants No. JP24K06878, No. JP24K00563, No. JP24K02948, and No. JP23K22492, and CSIS in Tohoku University.

DATA AVAILABILITY

No data were created or analyzed in this study.

APPENDIX A: SYMMETRY OPERATIONS

The eigenstates of our model can be characterized by various operators commuting or anticommuting with the Hamiltonian. We define the following four operators:

$$P = \sigma^z_A \sigma^z_{C_1} \sigma^z_{C_2} \sigma^z_B, \tag{A1}$$

$$Q = \sigma^z_A \sigma^z_{C_1} \sigma^x_{C_2}, \tag{A2}$$

$$R = \sigma^x_{C_1} \sigma^x_{C_2}, \tag{A3}$$

$$S = \sigma^x_A \sigma^y_{C_1} \sigma^x_{C_2} \sigma^y_B, \tag{A4}$$

where we find $[P, H] = 0$, $[Q, H] = 0$, $\{P, Q\} = 0$, $[R, H] = 0$, $[R, P] = 0$, $\{R, Q\} = 0$, $\{S, H\} = 0$, $[P, S] = 0$, $P^2 = 1$, $Q^2 = 1$, $R^2 = 1$, and $S^2 = 1$. The operator P is the parity operator for the number of Jordan-Wigner fermions with eigenvalues ± 1, and the total Hilbert space is devided into two subspaces with even or odd numbers of Jordan-Wigner fermions. The operator Q represents parity change, and the different-parity states degenerate due to $[Q, H] = 0$. We only treat the eigenstates $|\Psi_+\rangle$ in the even-parity sector ($H|\Psi_+\rangle = E|\Psi_+\rangle$, $P|\Psi_+\rangle = |\Psi_+\rangle$) in the main text. The operator R has the eigenvalues ± 1 (we shortly call it as R parity), and can be efficiently used for identifying the eigenstates. The operator S corresponds to spin inversion, and the spectra are symmetric with respect to the negative and positive sides in a specific parity sector.

The Jordan-Wigner representation of the operator R is given by $R = \sigma^x_{C_1}\sigma^x_{C_2} = (f^\dagger_{C_1} - f_{C_1})(f^\dagger_{C_2} + f_{C_2})$. The eigenstates of R are summarized as follows:

$$R(|eeff\rangle \pm |efef\rangle) = \pm(|eeff\rangle \pm |efef\rangle), \tag{A5}$$

$$R(|ffee\rangle \pm |fefe\rangle) = \pm(|ffee\rangle \pm |fefe\rangle), \tag{A6}$$

$$R(|ffff\rangle \pm |feef\rangle) = \pm(|ffff\rangle \pm |feef\rangle), \tag{A7}$$

$$R(|eeee\rangle \pm |effe\rangle) = \pm(|eeee\rangle \pm |effe\rangle), \tag{A8}$$

where we take the duplicate signs in the same order. The general eigenstates in the even-parity sector can be represented as

$$\begin{aligned}|\Psi_+\rangle =& a_1(|eeff\rangle + r|efef\rangle) + a_2(|ffff\rangle + r|feef\rangle) \\ &+ \lambda a_1(|ffee\rangle + r|fefe\rangle) + a_3(|eeee\rangle + r|effe\rangle),\end{aligned} \tag{A9}$$

where r $(=\pm 1)$ is the eigenvalue of R, λ $(=\pm 1)$ is the eigenvalue of space inversion, and parameters a_i $(i=1,2,3)$ are determined by solving $H|\Psi_+\rangle = E|\Psi_+\rangle$ and by the normalization condition (we do not explicitly introduce the space-inversion operator, since it is not easy to write it by the Pauli matrices).

Furthermore, we introduce the operator

$$Q\sigma_A^x = i\sigma_A^y\sigma_{C_1}^z\sigma_{C_2}^x. \tag{A10}$$

This operator commutes with H for $h=0$. A remarkable property of this operator is to satisfy $\{Q\sigma_A^x, R\}=0$ and $[Q\sigma_A^x, P]=0$. The state $Q\sigma_A^x|\Psi_+\rangle$ degenerates with $|\Psi_+\rangle$, but the eigenvalue of R for $Q\sigma_A^x|\Psi_+\rangle$ is different from that for $|\Psi_+\rangle$. Thus, R identifies the degeneracy at $h=0$. Because of the R-parity change, we obtain $\langle\Psi_+|Q\sigma_A^x|\Psi_+\rangle = 0$.

APPENDIX B: DERIVATION OF $\Delta E_B^{\max}$ AND $\Delta E_{B,B}^{\max}$

Let us derive the maximum of ΔE_B, $\Delta E_B^{\max}$. For this purpose, we first transform ΔE_B into the following form:

$$\Delta E_B = \sqrt{W_0^2+X_0^2}\cos(2\theta+\delta_0) - |W_0|, \tag{B1}$$

where

$$W_0 = \left(1-s_z^2\right)\epsilon_B + \left(1-s_x^2\right)\epsilon_R, \tag{B2}$$

$$X_0 = r_x s_y (kC_{AR} - hC_{AB}) + r_y s_x h D_{AB}, \tag{B3}$$

and the phase factor δ_0 is determined by the relations

$$\cos\delta_0 = \frac{-W_0}{\sqrt{W_0^2+X_0^2}}, \tag{B4}$$

$$\sin\delta_0 = \frac{-X_0}{\sqrt{W_0^2+X_0^2}}. \tag{B5}$$

We find

$$\Delta E_B \leqslant \sqrt{W_0^2+X_0^2} - |W_0|, \tag{B6}$$

and $\Delta E_B^{\max}$ is obtained for $2\theta+\delta_0=0$. The RHS of Eq. (B6) is a function of $\vec{r}$ and $\vec{s}$, which are determined to maximize ΔE_B. Hereafter, $\vec{r}$ and $\vec{s}$ are respectively parametrized as $\vec{r} = (\sin\mu\cos\nu, \sin\mu\sin\nu, \cos\mu)$ and $\vec{s} = (\sin\xi\cos\eta, \sin\xi\sin\eta, \cos\xi)$. The factor W_0 is represented as

$$W_0 = \epsilon_B\sin^2\xi + \epsilon_R(1-\sin^2\xi\cos^2\eta). \tag{B7}$$

According to $\alpha = 2k/(\epsilon+k-2h)$ and $\beta = 2k/(\epsilon+k+2h)$, we find $k(\alpha-\beta) = 2h\alpha\beta$, and this equation is transformed into

$$kC_{AR} - hC_{AB} = -hD_{AB}. \tag{B8}$$

Thus, the factor X_0 is represented as

$$X_0 = (r_y s_x - r_x s_y)hD_{AB} = hD_{AB}\sin\mu\sin\xi\sin(\nu-\eta). \tag{B9}$$

The RHS of Eq. (B6) is an increasing function of $\sin^2\xi$, and is maximized for $\xi=\pi/2$. After that, we obtain $W_0 = \epsilon_B + \epsilon_R\sin^2\eta$ and $X_0 = hD_{AB}\sin\mu\sin(\nu-\eta)$. The η dependence of X_0 can be absorbed by the optimization of ν, and thus, we can determine η to optimize W_0. The RHS of Eq. (B6) is a decreasing function of $|W_0|$. Since ϵ_B and ϵ_R are negative, we take $\eta=0$. The RHS of Eq. (B6) is an increasing function of $|X_0|$, and thus we take $\mu=\nu=\pi/2$. Finally, we obtain Eq. (17).

We also derive the maximum value of $\Delta E_{B,B}$, $\Delta E_{B,B}^{\max}$. For this purpose, we transform $\Delta E_{B,B}$ into the following form:

$$\Delta E_{B,B} = \sqrt{W^2+X^2}\cos(2\theta+\delta) - |W|, \tag{B10}$$

where

$$W = \epsilon_B\left(1-s_z^2\right) = \epsilon_B\sin^2\xi, \tag{B11}$$

$$\begin{aligned} X &= -h(r_x s_y C_{AB} - r_y s_x D_{AB}) \\ &= -4Z^2 h\sin\mu\sin\xi\{\sin(\eta-\nu) + \alpha\beta\sin(\eta+\nu)\}, \end{aligned} \tag{B12}$$

and the phase factor δ is determined from the the relations

$$\cos\delta = \frac{-W}{\sqrt{W^2+X^2}}, \tag{B13}$$

$$\sin\delta = \frac{-X}{\sqrt{W^2+X^2}}. \tag{B14}$$

We find

$$\Delta E_{B,B} \leqslant \sqrt{W^2+X^2} - |W|, \tag{B15}$$

and $\Delta E_{B,B}^{\max}$ is obtained for $2\theta+\delta=0$. The RHS of Eq. (B15) is to be maximized with respect to $\vec{r}$ and $\vec{s}$. The RHS of Eq. (B15) is an increasing function of $\sin^2\xi$, and we take $\xi=\pi/2$. Then, the RHS of Eq. (B15) is maximized for the maximum value of $|X|$. We take $\mu=\eta=\pi/2$ and $\nu=0$, since $\alpha\beta>0$. Finally, we obtain Eq. (19).

APPENDIX C: EFFECT OF DEGENERACY BETWEEN EVEN- AND ODD-PARITY STATES

In the main text, we focused on the lowest-energy state $|\psi\rangle$ in the even-parity sector. The state $|\psi\rangle$ degenerates with $|\phi\rangle = Q|\psi\rangle$ in the odd-parity sector. Here, we check whether our result holds in the odd-parity sector. For this purpose, we can use the following transformation $[P_A(n) = (I_A + n\vec{r}\cdot\vec{\sigma}_A)/2]$:

$$QP_A(n)Q = P_A(-n) \quad (r_z=0), \tag{C1}$$

$$QU_B(n)Q = U_B(n), \tag{C2}$$

$$Q(ib_Ab_B)Q = ib_Ab_B, \tag{C3}$$

$$Q(ic_Ac_B)Q = ic_Ac_B, \tag{C4}$$

where $Qb_iQ = -b_i$ and $Qc_iQ = -c_i$ $(i=A,B)$. We find

$$\langle\phi|ib_Ab_B|\phi\rangle = \langle\psi|ib_Ab_B|\psi\rangle, \tag{C5}$$

$$\langle\phi|ic_Ac_B|\phi\rangle = \langle\psi|ic_Ac_B|\psi\rangle. \tag{C6}$$

Thus, the b- and c-Majorana correlators are equivalent in both even- and odd-parity sectors. We also find that Q changes the sign of n in Eq. (C1). The QET performance at least for $r_z=0$ is not affected by the parity change, since the sign change in Eq. (C1) can be absorbed by that of r_x and r_y.

It would be helpful for readers to mention fourfold degeneracy of the lowest-energy eigenstates for $h = 0$. The eigenstates are identified with the signs of the eigenvalues of P and R where the eigenvalue of P is denoted as p ($= \pm 1$). The eigenstates are specified as $|+,+\rangle = |\psi\rangle$, $|+,-\rangle = Q\sigma_A^x|\psi\rangle$, $|-,+\rangle = b_A|\psi\rangle$, and $|-,-\rangle = Q|\psi\rangle = |\phi\rangle$, where the two signs in $|\pm,\pm\rangle$ correspond to the signs of p and r from the left. Then, we find

$$\langle p, r|ib_Ab_B|p, r\rangle = -prC_{AB}, \tag{C7}$$

$$\langle p, r|ic_Ac_B|p, r\rangle = D_{AB}. \tag{C8}$$

Therefore, at least for $h = 0$, the absolute values of the b- and c-Majorana correlators do not change for any combination of p and r.

APPENDIX D: ON THE MINIMIZATION IN EQ. (28)

We show some details about the minimization in Eq. (28). For general $P_A(n) = (I_A + n\vec{r}\cdot\vec{\sigma}_A)/2$, the reduced density matrix $\rho_B^{\rm m}(n)$ is given by

$$\rho_B^{\rm m}(n) = (1-\zeta)|e\rangle\langle e| + \kappa|e\rangle\langle f| + \kappa^*|f\rangle\langle e| + \zeta|f\rangle\langle f|, \tag{D1}$$

where ζ and κ are respectively defined by

$$\zeta = \frac{2Z^2((1-nr_z)+\alpha^2(1+nr_z))}{1+2nr_z(\alpha^2-\beta^2)Z^2}, \tag{D2}$$

$$\kappa = \frac{2nZ^2((r_x+ir_y)+\alpha\beta(r_x-ir_y))}{1+2nr_z(\alpha^2-\beta^2)Z^2}. \tag{D3}$$

The eigenvalues of $\rho_B^{\rm m}(n)$ are given by

$$\lambda_\pm^{\rm m}(n) = \tfrac{1}{2}(1 \pm \sqrt{1-4\zeta(1-\zeta)+4|\kappa|^2}). \tag{D4}$$

We find that $\lambda_\pm^{\rm m}(n)$ depend on both n and $\vec{r}$. Furthermore, we find

$$p_n = \tfrac{1}{2}(1+2nr_z(\alpha^2-\beta^2)Z^2), \tag{D5}$$

and p_n also depends on n. We examine $\sum_n p_n S(\rho_B^{\rm m}(n))$ as functions of h/k and $\vec{r}$. We have confirmed numerically that $\sum_n p_n S(\rho_B^{\rm m}(n))$ is minimized for $r_x = 1$. Therefore, it is reasonable to take $P_A(n) = (I_A + n\sigma_A^x)/2$.

APPENDIX E: PROOF OF EQUALITY BETWEEN EQ. (19) AND THE RHS OF EQ. (25) FOR OPTIMIZED $P_A(n)$

The equality between Eq. (19) and the RHS of Eq. (25) for optimized $P_A(n)$ is derived by using $\beta_{\rm eff}$ that is a unique solution of Eq. (28).

For the derivation of $\beta_{\rm eff}$, let us start with $\rho_B^{\rm i}$ and $\rho_B^{\rm m}(n)$ that are respectively evaluated as

$$\rho_B^{\rm i} = 2Z^2[(1+\beta^2)|e\rangle\langle e| + (1+\alpha^2)|f\rangle\langle f|], \tag{E1}$$

$$\rho_B^{\rm m}(n) = 2Z^2[(1+\beta^2)|e\rangle\langle e| + (1+\alpha^2)|f\rangle\langle f| + n(1+\alpha\beta)(|e\rangle\langle f| + |f\rangle\langle e|)]. \tag{E2}$$

A remarkable property of $\rho_B^{\rm m}(n)$ is that the eigenvalues, $\lambda_\pm^{\rm m}$, do not depend on n:

$$\lambda_\pm^{\rm m} = \tfrac{1}{2}(1 \pm \sqrt{1-16Z^4(\alpha-\beta)^2}) \equiv \tfrac{1}{2}(1 \pm g). \tag{E3}$$

Thus, $I_{\rm QC}$ is simply represented as $I_{\rm QC} = S(\rho_B^{\rm i}) - S(\rho_B^{\rm m}(n))$. Since $\lambda_\pm^{\rm m}$ is independent of n, Eq. (28) is reduced to $S(\sigma_B) = S(\rho_B^{\rm m}(n))$ for the optimized $P_A(n)$. Then, we can solve Eq. (28) for $\beta_{\rm eff}$ by just comparing the eigenvalues of σ_B with $\lambda_\pm^{\rm m}$. We find

$$\beta_{\rm eff} h = \log\sqrt{\lambda_+^{\rm m}/\lambda_-^{\rm m}}. \tag{E4}$$

Let us compare $\Delta E_{B,B}^{\max}$ in Eq. (19) with the RHS of Eq. (25). For this purpose, we transform the RHS into the following form:

$$\mathcal{F}\big(\rho_B^{\rm i}; H_B\big) - F(\sigma_B) + \frac{1}{\beta_{\rm eff}} I_{\rm QC} = \epsilon_B + \frac{h}{\log\sqrt{\lambda_+^{\rm m}/\lambda_-^{\rm m}}}\big(\log Z_{\rm eff} - S\big(\rho_B^{\rm m}\big)\big), \tag{E5}$$

where the partition function is evaluated as $Z_{\rm eff} = {\rm tr}_B e^{-\beta_{\rm eff}H_B} = 1/\sqrt{\lambda_+^{\rm m}\lambda_-^{\rm m}}$. We can analytically show

$$\sqrt{\Big(\frac{\epsilon_B}{h}\Big)^2 + C_{AB}^2} = \sqrt{(2Z^2(\alpha^2-\beta^2))^2 + (4Z^2(1+\alpha\beta))^2} = 2Z^2\sqrt{4+8\alpha\beta+(\alpha^2+\beta^2)^2} = g, \tag{E6}$$

and

$$\frac{\log Z_{\rm eff} - S\big(\rho_B^{\rm m}(n)\big)}{\log\sqrt{\lambda_+^{\rm m}/\lambda_-^{\rm m}}} = \frac{-\log\sqrt{\lambda_+^{\rm m}\lambda_-^{\rm m}} + \lambda_+^{\rm m}\log\lambda_+^{\rm m} + \lambda_-^{\rm m}\log\lambda_-^{\rm m}}{\log\sqrt{\lambda_+^{\rm m}/\lambda_-^{\rm m}}} = \frac{-\log\sqrt{\lambda_+^{\rm m}\lambda_-^{\rm m}} + \frac{1}{2}(1+g)\log\lambda_+^{\rm m} + \frac{1}{2}(1-g)\log\lambda_-^{\rm m}}{\log\sqrt{\lambda_+^{\rm m}/\lambda_-^{\rm m}}} = g. \tag{E7}$$

Therefore, the equality between $\Delta E_{B,B}^{\max}$ in Eq. (19) and the RHS of Eq. (25) is confirmed by our optimized $P_A(n)$.

[1] C. H. Bennett, G. Brassard, C. Crepeau, R. Jozsa, A. Peres, and W. K. Wootters, Teleporting an unknown quantum state via dual classical and Einstein-Podolsky-Rosen channels, Phys. Rev. Lett. **70**, 1895 (1993).

[2] L. Susskind and Y. Zhao, Teleportation through the wormhole, Phys. Rev. D **98**, 046016 (2018).

[3] T. Schuster, B. Kobrin, P. Gao, I. Cong, E. T. Khabiboulline, N. M. Linke, M. D. Lukin, C. Monroe, B. Yoshida, and

N. Y. Yao, Many-body quantum teleportation via operator spreading in the traversable wormhole protocol, Phys. Rev. X **12**, 031013 (2022).
[4] D. Jafferis, A. Zlokapa. J. D. Lykken, D. K. Kolchmeyer, S. I. Davis, N. Lauk, H. Neven, and M. Spiropulu, Traversable wormhole dynamics on a quantum processor, Nature (London) **612**, 51 (2022).
[5] A. Milekhin and F. K. Popov, Measurement-induced phase transition in teleportation and wormholes, SciPost Phys. **17**, 020 (2024).
[6] A. Kitaev, Anyons in an exactly solved model and beyond, Ann. Phys. **321**, 2 (2006).
[7] Z. Nussinov and J. van den Brink, Compass models: Theory and physical motivations, Rev. Mod. Phys. **87**, 1 (2015).
[8] M. Hermanns, I. Kimchi, and J. Knolle, Physics of the Kitaev model: Fractionalization, dynamic correlations, and material connections, Annu. Rev. Condens. Matter Phys. **9**, 17 (2018).
[9] J. Knolle and R. Moessner, A field guide to spin liquids, Annu. Rev. Condens. Matter Phys. **10**, 451 (2019).
[10] H. Takagi, T. Takayama, G. Jackeli, G. Khaliullin, and S. E. Nagler, Concept and realization of Kitaev quantum spin liquids, Nat. Rev. Phys. **1**, 264 (2019).
[11] L. Janssen and M. Vojta, Heisenberg–Kitaev physics in magnetic fields, J. Phys.: Condens. Matter **31**, 423002 (2019).
[12] Y. Motome and J. Nasu, Hunting Majorana fermions in Kitaev magnets, J. Phys. Soc. Jpn. **89**, 012002 (2020).
[13] C. Hickey and S. Trebst, Kitaev materials, Phys. Rep. **950**, 1 (2022).
[14] T. Minakawa, Y. Murakami, A. Koga, and J. Nasu, Majorana-mediated spin transport in Kitaev quantum spin liquids, Phys. Rev. Lett. **125**, 047204 (2020).
[15] A. Koga, Y. Murakami, and J. Nasu, Majorana correlations in the Kitaev model with ordered-flux structures, Phys. Rev. B **103**, 214421 (2021).
[16] H. Taguchi, Y. Murakami, A. Koga, and J. Nasu, Role of Majorana fermions in spin transport of anisotropic Kitaev model, Phys. Rev. B **104**, 125139 (2021).
[17] J. Nasu, Y. Murakami, and A. Koga, Scattering phenomena for spin transport in a Kitaev spin liquid, Phys. Rev. B **106**, 024411 (2022).
[18] T. Misawa, J. Nasu, and Y. Motome, Interedge spin resonance in the Kitaev quantum spin liquid, Phys. Rev. B **108**, 115117 (2023).
[19] M. O. Takahashi, M. G. Yamada, M. Udagawa, T. Mizushima, S. Fujimoto, Nonlocal spin correlation as a signature of ising anyons trapped in vacancies of the Kitaev spin liquid, Phys. Rev. Lett. **131**, 236701 (2023).
[20] S. Vijay and L. Fu, Teleportation-based quantum information processing with Majorana zero modes, Phys. Rev. B **94**, 235446 (2016).
[21] L. Fu, Electron Teleportation via Majorana bound states in a mesoscopic superconductor, Phys. Rev. Lett. **104**, 056402 (2010).
[22] H.-L. Huang, M. Narozniak, F. Liang, Y. Zhao, A. D. Castellano, M. Gong, Y. Wu, S. Wang, J. Lin, Y. Xu, H. Deng, H. Rong, J. P. Dowling, C.-Z. Peng, T. Byrnes, X. Zhu, and J.-W. Pan, Emulating quantum teleportation of a Majorana zero mode qubit, Phys. Rev. Lett. **126**, 090502 (2021).
[23] M. Hotta, A protocol for quantum energy distribution, Phys. Lett. A **372**, 5671 (2008).
[24] M. Hotta, Quantum measurement information as a key to energy extraction from local vacuums, Phys. Rev. D **78**, 045006 (2008).
[25] M. Hotta, Quantum energy teleportation in spin chain systems, J. Phys. Soc. Jpn. **78**, 034001 (2009).
[26] M. Hotta, Energy entanglement relation for quantum energy teleportation, Phys. Lett. A **374**, 3416 (2010).
[27] J. Trevison and M. Hotta, Quantum energy teleportation across a three-spin Ising chain in a Gibbs state, J. Phys. A: Math. Theor. **48**, 175302 (2015).
[28] N. A. Rodríguez-Briones, H. Katiyar, E. Martin-Martinez, and R. Laflamme, Experimental Activation of Strong Local Passive States with Quantum Information, Phys. Rev. Lett. **130**, 110801 (2023).
[29] K. Ikeda, Demonstration of quantum energy teleportation on superconducting quantum hardware, Phys. Rev. Appl. **20**, 024051 (2023).
[30] K. Ikeda, Investigating global and topological orders of states by local measurement and classical communication: Study on SPT phase diagrams by quantum energy teleportation, AVS Quantum Sci. **5**, 035002 (2023).
[31] K. Itoh, Y. Masaki, and H. Matsueda, Quantum Energy Teleportation and Entropy Change due to Feedback Control in One-Dimensional Heisenberg Model, arXiv:2305.03967.
[32] J. Wang and S. Yao, Quantum Energy Teleportation versus Information Teleportation, Quantum **8**, 1564 (2024).
[33] T. Sagawa and M. Ueda, Second law of thermodynamics with discrete quantum feedback control, Phys. Rev. Lett. **100**, 080403 (2008).
[34] H. Tajima, Second law of information thermodynamics with entanglement transfer, Phys. Rev. E **88**, 042143 (2013).
[35] K. Funo, Y. Watanabe, and M. Ueda, Thermodynamic work gain from entanglement, Phys. Rev. A **88**, 052319 (2013).
[36] J. J. Park, K.-H. Kim, T. Sagawa, and S. W. Kim, Heat engine driven by purely quantum information, Phys. Rev. Lett. **111**, 230402 (2013).
[37] G. Manzano, F. Plastina, and R. Zambrini, Optimal Work Extraction and Thermodynamics of Quantum Measurements and Correlations, Phys. Rev. Lett. **121**, 120602 (2018).
[38] S. Minagawa, M. H. Mohammady, K. Sakai, K. Kato, and F. Buscemi, Universal validity of the second law of information thermodynamics, npj Quantum Information **11**, 18 (2025).
[39] K. Itoh, Y. Masaki, and H. Matsueda, Upper bound on locally extractable energy from entangled pure state under feedback control, arXiv:2408.11522.
[40] H. J. Groenewold, A problem of information gain by quantal measurements, Int. J. Theor. Phys. **4**, 327 (1971).
[41] M. Ozawa, On information gain by quantum measurements of continuous observables, J. Math. Phys. **27**, 759 (1986).